Biochemistry

Article

pubs.acs.org/biochemistry

Properties of Intermediates in the Catalytic Cycle of Oxalate Oxidoreductase and Its Suicide Inactivation by Pyruvate

Elizabeth Pierce,[†,∥] Steven O. Mansoorabadi,[‡] Mehmet Can,[†] George H. Reed,[§] and Stephen W. Ragsdale*[,†]

[†]Department of Biological Chemistry, University of Michigan, Ann Arbor, Michigan 48109-0606, United States
[‡]Department of Chemistry and Biochemistry, Auburn University, 179 Chemistry Building, Auburn, Alabama 36849, United States
[§]Department of Biochemistry, University of Wisconsin—Madison, 440 Henry Mall, Madison, Wisconsin 53726, United States

ABSTRACT: Oxalate:ferredoxin oxidoreductase (OOR) is an unusual member of the thiamine pyrophosphate (TPP)-dependent 2-oxoacid:ferredoxin oxidoreductase (OFOR) family in that it catalyzes the coenzyme A (CoA)-independent conversion of oxalate into 2 equivalents of carbon dioxide. This reaction is surprising because binding of CoA to the acyl-TPP intermediate of other OFORs results in formation of a CoA ester, and in the case of pyruvate:ferredoxin oxidoreductase (PFOR), CoA binding generates the central metabolic intermediate acetyl-CoA and promotes a 10^5-fold acceleration of the rate of electron transfer. Here we describe kinetic, spectroscopic, and computational results to show that CoA has no effect on catalysis by OOR and describe the chemical rationale for why this cofactor is unnecessary in this enzymatic transformation. Our results demonstrate that, like PFOR, OOR binds pyruvate and catalyzes decarboxylation to form the same hydroxyethylidine−TPP (HE−TPP) intermediate and one-electron transfer to generate the HE−TPP radical. However, in OOR, this intermediate remains stranded at the active site as a covalent inhibitor. These and other results indicate that, like other OFOR family members, OOR generates an oxalate-derived adduct with TPP (oxalyl-TPP) that undergoes decarboxylation and one-electron transfer to form a radical intermediate remaining bound to TPP (dihydroxymethylidene−TPP). However, unlike in PFOR, where CoA binding drives formation of the product, in OOR, proton transfer and a conformational change in the "switch loop" alter the redox potential of the radical intermediate sufficiently to promote the transfer of an electron into the iron−sulfur cluster network, leading directly to a second decarboxylation and completing the catalytic cycle.

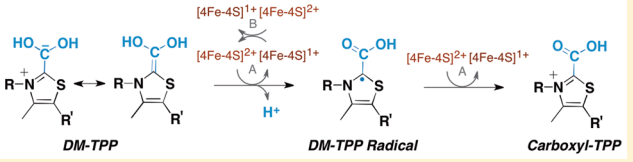

Oxalate:ferredoxin oxidoreductase (OOR) is an unusual member of the 2-oxoacid:ferredoxin oxidoreductase (OFOR) family (EC 1.2.7.11). Members of this family of enzymes use thiamine pyrophosphate (TPP) and [4Fe-4S] clusters to catalyze the oxidative decarboxylation of various substrates, such as pyruvate, 2-oxoglutarate, and 2-oxobutyrate (eq 1).[1,2] These reactions yield low-potential electrons that are transferred to ferredoxin, which serves as an intermediary carrier for microbial reactions that drive carbon, nitrogen, and hydrogen cycles, such as CO_2 fixation, hydrogen generation, and reduction of nitrogen to ammonia. Another product of the OFOR reactions is a "high-energy" acyl-CoA derivative, e.g., acetyl-CoA or succinyl-CoA. These products conserve the free energy of the substrate transformation and are linked to other important cellular reactions, such as ATP formation through substrate-level phosphorylation and the delivery of acetyl groups into the TCA cycle, fatty acid synthesis, and acetylcholine formation.

$$\mathrm{R{-}CO{-}COOH + CoA \rightarrow R{-}CO{-}CoA + CO_2 + 2H^+ + 2e^-}$$
$$\Delta E^{\circ\prime} \sim 515\ \mathrm{mV\ (R = CH_3)} \qquad (1)$$

What is unusual about OOR is that, unlike all other known members of the OFOR family, OOR does not use CoA; instead, OOR oxidizes oxalate directly to CO_2 (eq 2).[3,4] This was first indicated by studies with extracts from oxalate-grown cells of *Moorella thermoacetica*, which catalyzed oxalate-dependent benzyl viologen reduction with an activity that is only slightly stimulated by CoA, suggesting that *M. thermoacetica* catabolizes oxalate by a CoA-independent mechanism that does not use formate as an intermediate.[3,4] Via kinetic studies with the purified enzyme, the unusual CoA independence was confirmed[4] and forms the basis of the experiments described in this paper.[5,6]

$$\mathrm{C_2O_4^{2-} \rightarrow 2CO_2 + 2e^-} \quad \Delta E^{\circ\prime} = 492\ \mathrm{mV} \qquad (2)$$

The reverse reaction of OOR is an avenue for conversion of the greenhouse gas, CO_2, into nonvolatile oxalate ($C_2O_4^{2-}$). Oxalate, the most oxidized two-carbon compound, occurs naturally in high concentrations in some plants and fungi and plays important roles in calcium regulation and protection from and detoxification of heavy metals.[7,8] Microbes and plants then degrade oxalate by various aerobic reactions, including oxalate oxidase-catalyzed O_2-dependent conversion to CO_2 and H_2O_2,[9]

Received: March 10, 2017
Revised: May 16, 2017
Published: May 17, 2017

DOI: 10.1021/acs.biochem.7b00222
Biochemistry 2017, 56, 2824−2835

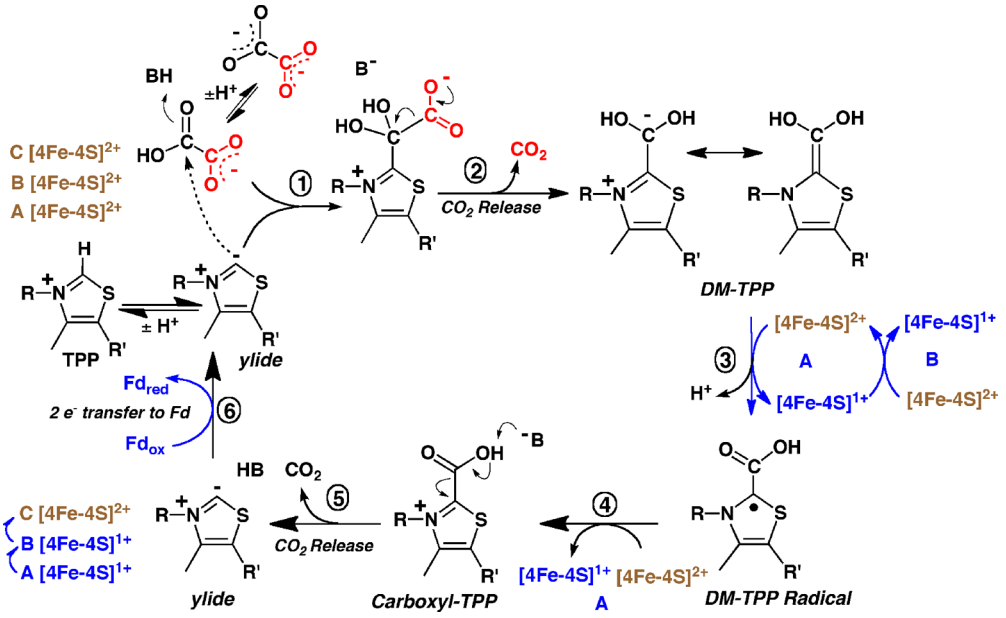

Figure 1. Proposed mechanism of OOR. See the text for details.

and conversion to CO_2 and formate by oxalate decarboxylase.[10] Before OOR was discovered, the only known anaerobic pathway for oxalate metabolism was via TPP-dependent oxalyl-CoA decarboxylase, which produces CO_2 and formyl-CoA.[11,12] Acetogenic bacteria like *M. thermoacetica* couple the Wood–Ljungdahl pathway (eq 3) to OOR to catalyze four cycles of oxalate oxidation, producing eight electrons, which are used to reduce two of the eight molecules of CO_2 formed to acetate (eq 4).[13,14] In *M. thermoacetica*, both OOR[15] and the Wood–Ljungdahl pathway[13] are induced by exposure to oxalate.

$$2CO_2 + 8H^+ + 8e^- \rightarrow CH_3COOH + 2H_2O \quad (3)$$

$$4C_2O_4^{2-} + 8H^+ \rightarrow 6CO_2 + CH_3COOH + 2H_2O \quad (4)$$

OOR and other well-characterized members of the OFOR family share between 35 and 60% sequence similarity. OOR has the highest degree of homology to archaeal and bacterial pyruvate:ferredoxin oxidoreductases (PFORs). For example, the *M. thermoacetica* OOR shares ~40% sequence similarity with the structurally characterized PFOR from *Desulfovibrio africanus*.[16] However, OOR consists of three separate peptides that dimerize to form a 260 kDa $(\alpha\beta\gamma)_2$ oligomer, while the *D. africanus* PFOR dimer consists of two identical 135 kDa peptides, in which the α, β, and γ subunits are fused.[4] Both PFOR and OOR contain (per 135 kDa unit) one TPP molecule, 1–2 equiv of Mg^{2+}, and three [4Fe-4S] clusters, a composition like that of most other members of the OFOR family.[4] Furthermore, a recent 2.27 Å resolution crystal structure of OOR reveals a striking resemblance between the OOR $(\alpha\beta\gamma)_2$ dimer and the PFOR α_2 dimer,[17] in which each monomeric (or heterotrimeric) unit contains a deeply buried TPP binding site (the active site) connected to the protein surface by an approximately linear arrangement of three [4Fe-4S] clusters. This active site is highly conserved except for substitutions that fine-tune OOR and PFOR for binding their preferred substrates[17] and the presence in OOR of positively charged and polar residues that drive catalysis through loop and side chain movements.[18]

Given the high degree of sequence and structural homology, one might expect OOR to have a mechanism similar to that of PFOR; however, unlike pyruvate and the other 2-oxoacid substrates of the OFOR enzymes, oxalate is a dicarboxylic acid without a ketone adjacent to the carboxylic acid group, making it significantly less electrophilic toward nucleophilic attack by TPP. However, the structures of covalent TPP–oxalate and TPP–CO_2 adducts strongly indicate that the OOR and PFOR mechanisms do indeed coincide, at least in the early CoA-independent steps.[18] One of the goals of this paper is to understand how OOR catalyzes TPP-dependent activation and C–C bond cleavage in the absence of the ketone functionality on the substrate and without the involvement of CoA.

Thus, our hypothesis is that the catalytic mechanism of OOR entails CoA-independent steps with counterparts in the PFOR mechanism.[2,19−21] In PFOR, as well as in pyruvate dehydrogenase and pyruvate decarboxylase, C2 of the thiazolium ring of TPP is deprotonated to form a carbanion that performs a nucleophilic attack on the α-keto group of pyruvate, releasing CO_2 and leaving the hydroxyethylidene–TPP (HE–TPP) intermediate. The HE–TPP intermediate transfers an electron into the [4Fe-4S] chain, producing the resonance-stabilized HE–TPP radical.[22] After formation of this radical, CoA plays a key role in the remaining steps of the PFOR mechanism. The HE–TPP radical intermediate is metastable. In the PFOR from *M. themoaceticum*, it decays slowly (with a half-life of ~4 min) in the absence of CoA; however, in the presence of CoA, the radical decays 10^5-fold more quickly.[20]

Addition of CoA to the HE–TPP radical intermediate results in a second electron transfer into the cluster network and formation of product acetyl-CoA. The mechanism by which CoA promotes this second electron transfer is unknown. Finally, the two electrons residing in the [4Fe-4S] clusters are transferred to the native electron acceptor, e.g., ferredoxin, or to an artificial electron acceptor, such as methyl viologen (MV).

A proposed catalytic mechanism for OOR (Figure 1) includes initial steps (1–3) similar to those just described for PFOR. On the basis of solution pK_a values of oxalate (1.3 and 3.8), the substrate is initially likely to carry two negative

DOI: 10.1021/acs.biochem.7b00222
Biochemistry 2017, 56, 2824–2835

charges. In step 1, protonation of one of the carboxylates promotes reaction of oxalate with C2 of TPP, followed by a second protonation to form oxalyl-TPP. In addition, the OOR active site contains positive charges, including Arg31α, and H-bond donors that could facilitate this nucleophilic attack and stabilize the TPP adduct.[17,18] In step 2, oxalyl-TPP undergoes decarboxylation, producing a dihydroxymethylidene−TPP (DM−TPP) intermediate, which would be in resonance with its zwitterionic form. Then, as in PFOR, one-electron transfer into the iron−sulfur cluster network would generate the DM−TPP radical (step 3). In step 4, one-electron oxidation of the DM−TPP radical yields carboxyl-TPP and sends another electron into the chain of iron−sulfur clusters. Thus, stepwise two-electron oxidation of DM−TPP generates carboxyl-TPP accompanied by reduction of two of the [4Fe-4S] clusters. How much of the DM−TPP radical accumulates would depend on the rate of these electron transfer reactions; for example, if the decay of the substrate-derived radical is very fast, there would be very little and perhaps undetectable amounts of that radical. In step 5, carboxyl-TPP would release CO_2 and regenerate the ylide to initiate the next round of catalysis.

This paper describes experiments aimed at testing the mechanism proposed for OOR and its similarities to that of PFOR. We provide further evidence that OOR does not catalyze the reaction of 2-oxoacid substrates with CoA. Although we have not observed the DM−TPP radical intermediate directly, OOR does form the HE−TPP radical with the inhibitor pyruvate. This HE−TPP radical intermediate does not turn over but remains bound as a dead-end complex. The results suggest that the nature of the substrate and the mechanism of kinetic coupling (in step 4) control the stability of the radical and provide evidence that any radical derived from oxalate would be more reactive than those derived from pyruvate or other singly negatively charged 2-oxoacids. Combined with recent structural information about OOR,[17,18] it appears that conformational changes, particularly related to the switch loop,[18] also promote substrate binding and reactivity.

EXPERIMENTAL PROCEDURES

Growth of *M. thermoacetica* and Protein Purification. *M. thermoacetica* ATCC 39073 was grown at 55 °C in a 10 L fermenter that was continually sparged with CO_2. The medium was described previously.[4] All cells used for OOR purification were grown on 20 mM glucose and 28 mM sodium oxalate. Cells were harvested during exponential growth by centrifugation under CO_2 or N_2 and stored at −80 °C until they were used.

All protein purification steps and subsequent enzymatic manipulations were performed in a Vacuum Atmospheres (Hawthorne, CA) anaerobic chamber maintained at <4 ppm of O_2. OOR was purified as described previously,[4] except that the red agarose step was omitted. At the end of the preparation, fractions containing OOR were pooled, buffer exchanged into 50 mM Tris-HCl (pH 8.1) with 2 mM DTT, and concentrated to 0.32 mM for storage. The specific activity of purified OOR measured at 25 °C was 0.04 unit mg^{-1}.

Preparation of Thionin-Oxidized OOR. Oxidized OOR (OOR_{ox}) was prepared by adding small aliquots of an approximately 20 mM thionin solution to a sample of 0.32 mM OOR with mixing after each addition. Thionin reduction of OOR took place within a few seconds of mixing. Thionin was added until no change in its color was seen upon further addition (i.e., the protein/thionin solution remained dark purple after mixing). Alternatively, aliquots of approximately 80 μM OOR were mixed with small amounts of thionin in a 0.2 cm path length cuvette, to achieve the desired oxidation state. Then, OOR was dialyzed against three changes of a 300-fold excess of 50 mM Tris-HCl (pH 8.0) with equilibration for at least 8 h in each change of buffer. After this dialysis, the ultraviolet−visible (UV−vis) spectrum of OOR showed no evidence of thionin contamination. The final dialysis buffer was saved for dilution of the enzyme and substrate in subsequent experiments. The activity of thionin-oxidized OOR was 0.02 unit mg^{-1}, while the activity of a sample of as-isolated OOR, dialyzed under the same conditions, was 0.04 unit mg^{-1}.

Enzyme Assays. OOR activity was measured in 50 mM Tris-HCl and 2 mM DTT (pH 8.0). Assays at 25 °C were performed in an anaerobic chamber, using a UV−vis spectrophotometer from Ocean Optics (Dunedin, FL). For steady state assays, 1 mM sodium oxalate and 10 mM MV were used and the reduction of MV was followed at 578 nm (ε_{578} = 9.7 mM^{-1} cm^{-1}). In all assays, calculations were based on the assumption that oxidation of 1 mol of oxalate produces 2 mol of reduced MV.

To measure the effect of pyruvate on OOR activity, 11 μM OOR_{ox} was mixed with 1 mM pyruvate in 50 mM Tris-HCl (pH 8.0) and the UV−vis absorbance spectrum was monitored during the reaction. On the basis of the extent of reduction of the [4Fe-4S] clusters, the reaction of OOR with pyruvate reached equilibrium within 2 h. Before the enzyme was assayed, excess pyruvate was removed by concentrating and diluting OOR in 50 mM Tris-HCl (pH 8.0) using 10 kDa molecular weight cutoff microcentrifuge concentrators (Millipore, Billerica, MA), with six cycles of 9-fold concentration and dilution in fresh buffer. The activity of pyruvate-incubated OOR was measured as described above and was compared to the activities of a sample of OOR_{ox} incubated for the same time in 1 mM oxalate and a sample of OOR_{ox}, both buffer exchanged in the same way.

To measure the effect of oxalate on PFOR activity, PFOR (2.6 μg) was added to a solution containing 2 mM DTT, 1 mM TPP, 10 mM oxidized MV, 1 mM CoA, and 0.5 M Tris-HCl buffer (pH 7.6) in the absence of magnesium (to avoid interaction between oxalate and magnesium). Enzyme activities were calculated by following changes in absorbance at 578 nm, assuming an extinction coefficient of 9.78 mM^{-1} cm^{-1} and the reduction of two MV molecules per pyruvate. Only initial absorbance values of ≤0.2 were used to calculate the initial enzymatic rates. Before PFOR activity assays were performed, the PFOR stock was incubated in 2 mM DTT, 2 mM $MgCl_2$, 1 mM TPP, and 50 mM Tris-HCl (pH 7.6). To determine the steady state kinetic parameters (V_{max} and K_m), the pyruvate concentration was varied between 0.05 and 4 mM. To determine if PFOR can utilize oxalate as a substrate, a similar assay was performed with 10 mM oxalate in place of pyruvate and with 51 μg of PFOR. The oxalate inhibition assays were performed at a subsaturating concentration of pyruvate (0.2 mM) at oxalate concentrations of ≤40 mM and with 2.0 μg of PFOR.

UV−Vis Spectroscopy. OOR was diluted to approximately 4 μM in 50 mM Tris-HCl (pH 8.0) with or without 2 mM DTT. The enzyme was reduced at 25 °C by adding 100 μM sodium oxalate or 5−10 μM sodium dithionite. To measure the spectrum of the oxidized protein, OOR was oxidized with thionin and dialyzed, as described above.

DOI: 10.1021/acs.biochem.7b00222
Biochemistry 2017, 56, 2824−2835

EPR Spectroscopy. The EPR spectrum of as-isolated OOR was measured to determine the number of reactive iron−sulfur clusters and to test if substrate-derived radicals could be detected after incubation with oxalate or with pyruvate. Comparison of the UV−vis spectrum of as-isolated OOR with that of dithionite-reduced OOR showed that, when purified under anaerobic conditions, the as-isolated protein already had approximately 1.8 reduced $[4Fe\text{-}4S]^{+}$ clusters per monomer. In the presence of sodium oxalate (100 μM, final concentration), all three clusters in the protein underwent reduction. EPR spectra were recorded at 9 K with the instrumental parameters provided in the corresponding figure legends. The double integrals of the EPR signals were compared to that of a 1 mM copper(II) perchlorate standard to determine the number of spins per monomeric unit.

To observe and characterize the pyruvate-derived radical on OOR, 0.20 mM OOR was mixed with 1 mM unlabeled pyruvate or [3-$^{2}H_3$]pyruvate and incubated at 25 °C for 90 min. Each sample was split in half, and 1 mM CoA was added to one part of the sample. Samples were frozen after incubation for an additional 10 min. EPR instrumental parameters are provided in the corresponding figure legends.

Calculation of Redox Potentials and pK_a Values for OOR and PFOR Intermediates. Estimates for reduction potentials (vs the standard hydrogen electrode) and pK_a values for putative intermediates in the catalytic cycles of OOR and PFOR were calculated using density functional theory (DFT) as implemented in the Gaussian 98 software package.[23] The geometry of each intermediate was optimized using the Becke-style three-parameter Lee−Yang−Parr correlation functional (B3LYP) and Pople's diffuse polarized triple-ζ 6-311+G(d,p) basis set.[24,25] Vibrational frequency calculations were performed with the same level of theory at 298.15 K and 1.000 atm, using a scale factor of 0.9877.[26] Solvation energies of the intermediates in acetonitrile (for reduction potentials) and water (for pK_a values) were calculated using the polarizable continuum model (PCM).[27] Thermodynamic (Born−Haber) cycles were then constructed using the resulting Gibbs free energies to calculate the overall Gibbs free energy changes for the reduction and acid dissociation reactions, which were then converted to reduction potentials and pK_a values, respectively. For the pK_a estimates, a proton solvation free energy of −264.0 kcal/mol was utilized in the calculation.[28] Several studies have shown that the reduction potentials of diverse organic molecules calculated using the B3LYP functional in combination with PCM solvation show strong linear correlations with their experimental values.[29−32] Thus, reasonably accurate theoretical estimates of reduction potentials can be obtained with this protocol by applying a linear correction using the calculated and experimental values of a series of reference compounds. The calculated potentials for the OOR and PFOR intermediates were corrected using a standard curve obtained with calculated values for the reduction of oxygen ($O_2 + 4H_3O^+ + 4e^- \rightarrow 6H_2O$, and $O_2 + 2H_2O + 4e^- \rightarrow 4OH^-$) and hydrogen ($2H_3O^+ + 2e^- \rightarrow H_2 + 2H_2O$, and $2H_2O + 2e^- \rightarrow H_2 + 2OH^-$) and their corresponding experimental values versus the standard hydrogen electrode (1.229, 0.4, 0, and −0.8277 V, respectively). This amounted to a linear correction $E(\text{corr}) = 0.7499E(\text{calc}) - 3.547$, with an R^2 value of 0.9984 and a mean absolute error (MAE) of 0.026 V. Similarly, the pK_a values of the OOR and PFOR intermediates were calibrated using pK_a values calculated for H_3O^+, NH_4^+, and H_2O, and their corresponding experimental values (−1.74, 9.23, and 15.74, respectively). In this case, the correction was $pK_a(\text{corr}) = 0.9998pK_a(\text{calc}) - 0.7738$, with an R^2 value of 0.9996 and a MAE of 0.13.

Miscellaneous Methods. Protein concentrations were determined by the Rose Bengal method,[33] using a lysozyme standard. The concentration of TPP bound to OOR was determined by a fluorescent thiochrome assay,[34] using authentic purchased TPP as a standard. Metal concentrations were determined by ICP-OES at the Chemical Analysis Laboratory at the University of Georgia (Athens, GA). For metal and TPP analysis, 1.1 mL of 0.32 mM OOR was dialyzed against two changes of 850 mL of 50 mM Tris-HCl and 2 mM DTT (pH 8.0). Metal and TPP concentrations in the protein sample were calculated after subtracting the concentrations in a sample of the dialysis buffer treated exactly as was the protein. TPP and metal concentrations were similar to those found in a previous OOR preparation.[4]

RESULTS

Reaction of Pyruvate with OOR and Formation of a Pyruvate-Derived Radical on OOR. We previously showed that OOR can catalyze the oxidation of several 2-oxoacids besides oxalate. When OOR was mixed with 1 mM pyruvate and 10 mM MV, the amount of MV reduced approximated 2 mol/mol of dimeric OOR, suggesting that OOR may not be able to complete its catalytic cycle with pyruvate as a substrate.[4] Because the OOR catalytic cycle is hypothesized to contain intermediates covalently bound to TPP, we hypothesized that pyruvate may be a covalent inhibitor of OOR.

UV−vis spectroscopy showed that, while oxalate fully reduces all three iron−sulfur clusters of OOR, treatment with pyruvate led to only partial reduction of the clusters of either oxidized or partly reduced enzyme. When pyruvate was mixed with OOR, the decrease in absorbance at 420 nm, based on an extinction coefficient of 8.1 (nM cluster)$^{-1}$cm^{-1},[4] was equivalent to reduction of 8 and 26% of the clusters in two samples of as-isolated OOR from separate preparations and to 16% of the iron−sulfur clusters in a sample of thionin-oxidized OOR from the second preparation (Figure 2). Thus, although the redox potential of the (CO_2 + acetyl-CoA)/pyruvate couple (−0.515 V) is similar to that for the 2CO_2/oxalate (−0.492 V)

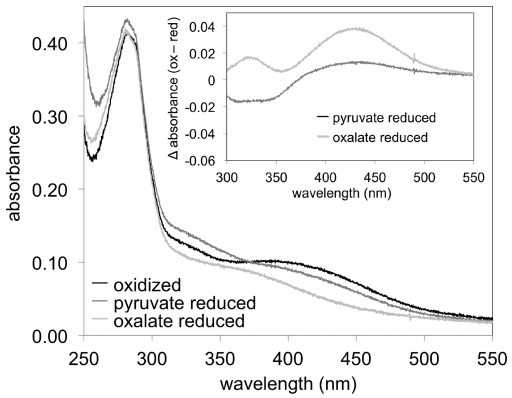

Figure 2. UV−vis spectra of pyruvate- and oxalate-reduced OOR. Eight micromolar OOR_{ox} (darkest line) was incubated with 1 mM pyruvate (lighter line) or oxalate (lightest line) until no further change in either spectrum was seen. The inset shows the difference spectra (oxidized − reduced) for both the oxalate-reduced and the pyruvate-reduced protein.

DOI: 10.1021/acs.biochem.7b00222
Biochemistry 2017, 56, 2824−2835

half-reaction,[5,6] pyruvate effects only a partial reduction of the clusters of OOR. Furthermore, while the absorbance in the 300−400 nm region decreases when OOR is reacted with oxalate or dithionite, it increases when the enzyme is reacted with pyruvate (Figure 2). Circular dichroism studies with other TPP-dependent enzymes have shown that TPP-bound intermediates give rise to spectral changes in the 350 nm region.[35] Similarly, when 2-oxoglutarate dehydrogenase is reacted with 2-oxoglutarate, a peak centered at 348−351 nm appears, which was assigned to a TPP−enamine intermediate.[36] Thus, this increase in absorbance in the 350 nm region when OOR is reacted with pyruvate may derive from this TPP-bound intermediate.

The reactions of OOR with oxalate, dithionite, and pyruvate were also monitored by EPR spectroscopy to obtain more information about how pyruvate and oxalate affect the iron−sulfur clusters and the TPP cofactor. On the basis of results of EPR spectroscopic experiments at 10 K, where the unpaired electron spins of the $[4Fe\text{-}4S]^{+}$ clusters can be monitored, when OOR was mixed with pyruvate, only a fraction of the iron−sulfur clusters underwent reduction (Figures 3 and 4). In contrast, when the enzyme reacts with oxalate, the clusters are fully reduced.[4] Moreover, the EPR spectrum of pyruvate-incubated OOR at 70 K exhibits the classic, signature pattern of the HE−TPP radical, whereas no signal corresponding to a radical is observed upon incubation of OOR with oxalate (Figure 5). In separate experiments with pyruvate, 6 and 15% of the iron−sulfur clusters were reduced. In these same experiments, the radical spectrum measured at 70 K corresponded to 0.08 and 0.2 spin mol^{-1}, respectively. The HE−TPP radical signal is observed when PFOR is mixed with pyruvate in the absence of CoA.[22]

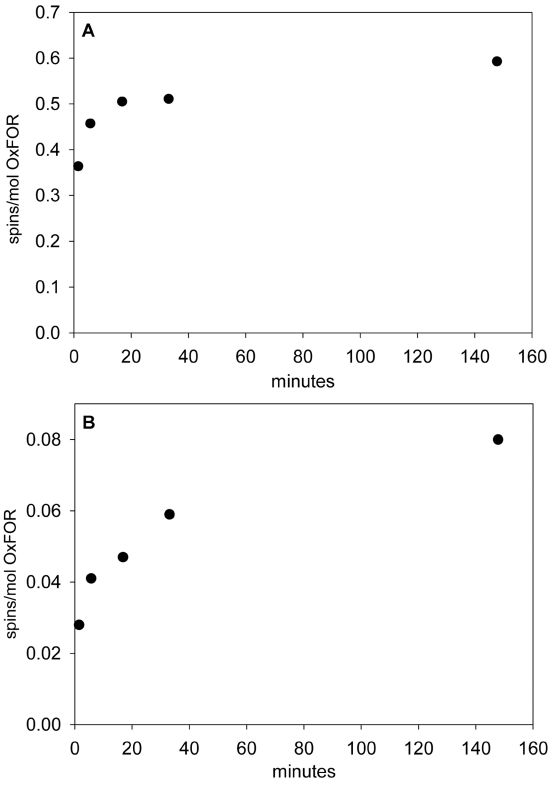

Figure 3. Quantitation of EPR signals produced when as-isolated (partly reduced) OOR was incubated with 1 mM pyruvate. OOR (38 μM) was mixed with 1 mM pyruvate in 50 mM Tris-HCl (pH 8.1). EPR samples were frozen after 1.5, 6, 17, 33, and 148 min. EPR spectra were integrated, and concentrations were calculated by comparison to a 1 mM copper perchlorate standard. (A) Amounts of $[4Fe\text{-}4S]^{+}$ clusters. Spectra were measured at 10 K. Other EPR parameters were as follows: receiver gain, 2×10^{3}; modulation frequency, 100 kHz; modulation amplitude, 10 G; center field, 3500 G; sweep width, 2000 G; microwave power, 0.103 mW. (B) Amounts of the pyruvate-derived radical. Spectra were measured at 70 K. Other EPR parameters were as follows: receiver gain, 2×10^{4}; modulation frequency, 100 kHz; modulation amplitude, 10 G; center field, 3500 G; sweep width, 2000 G; microwave power, 0.515 mW.

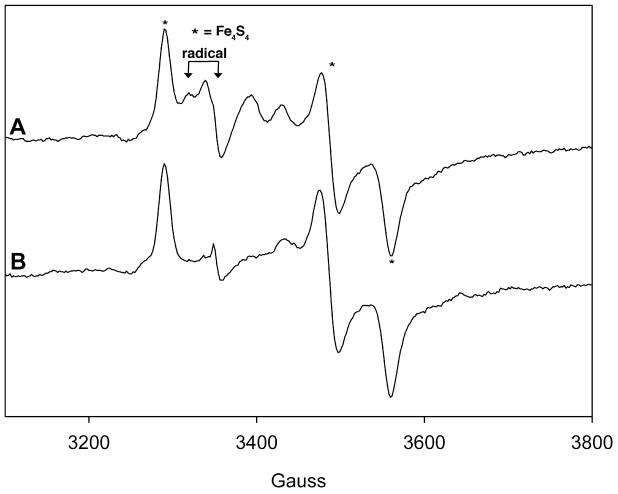

Figure 4. EPR spectra of as-isolated, partly reduced OOR and of OOR incubated with pyruvate, measured at 10 K. (A) OOR (38 μM) was mixed with 1 mM pyruvate in 50 mM Tris-HCl (pH 8.1). The sample was incubated at 25 °C and frozen 17 min after being mixed. (B) OOR (38 μM) in its as-isolated oxidation state, diluted in 50 mM Tris-HCl (pH 8.1). EPR parameters are the same as for Figure 3A.

Figure 3 shows the increase in the concentration of the HE−TPP radical over time as OOR is incubated with 1 mM pyruvate. To test the hypothesis that the signal derives from a pyruvate-based radical, we reacted OOR with isotopically labeled pyruvate. When OOR is incubated with $[3\text{-}^{2}H_{3}]$-pyruvate, resolved hyperfine splittings in the radical spectrum are lost (Figure 5). Similar results were observed when PFOR was treated with $[3\text{-}^{2}H_{3}]$pyruvate versus unlabeled pyruvate. Unlike in PFOR, where addition of CoA increases the rate of decay of the radical by 10^{5}-fold, addition of CoA to OOR and pyruvate mixtures 10 min before samples were frozen had no effect on the amplitude of the EPR signal of the radical.

To test the hypothesis that pyruvate is a covalent modifier (mechanism-based inhibitor) of OOR, pyruvate and oxalate were reacted together with OOR. After incubation with 1 mM pyruvate for 20 h and buffer exchange to remove excess pyruvate, the activity of OOR was reduced 8-fold (to 0.002 ± 0.0006 unit mg^{-1}) relative to that of untreated, buffer-exchanged OOR (0.02 ± 0.001 unit mg^{-1}). Assuming that inhibition is due to formation of the covalent adduct of pyruvate with TPP, the EPR measurements indicate that 14% of the enzyme is in the HE−TPP radical state (averaging the two experiments described above), which would also have a single reduced cluster. Then, on the basis of the EPR of the Fe−S clusters, 9% of the active sites would contain the "acetyl-TPP" form having two reduced clusters. This would leave 65% of the enzyme in the various other TPP adduct states, e.g., pyruvyl-TPP.

DOI: 10.1021/acs.biochem.7b00222
Biochemistry 2017, 56, 2824−2835

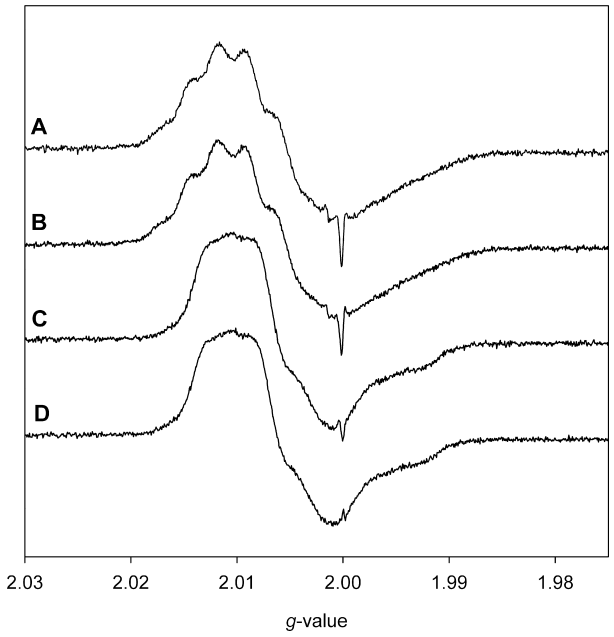

Figure 5. EPR spectrum of the pyruvate-derived radical on OOR. OOR (205 μM) was mixed with (A) 1 mM unlabeled pyruvate or (B) [3-$^2H_3$]pyruvate and incubated at 25 °C for 90 min. Each sample was split in half, and 1 mM CoA was added to one part of the sample [(C) unlabeled pyruvate with CoA and (D) [3-$^2H_3$]pyruvate with CoA]. Samples were frozen after being incubated for an additional 10 min. EPR parameters were as follows: receiver gain, 2×10^5; modulation frequency, 100 kHz; modulation amplitude, 0.4 G; center field, 3350 G; sweep width, 100 G; microwave power, 0.515 mW; temperature, 70 K. All four spectra have the same intensity scale. The sharp g = 2.00 feature is seen in spectra of the EPR cavity.

In our previous work, we showed that addition of CoA to assays of pyruvate oxidation coupled to MV reduction by OOR had no effect on the rate of the reaction.[4] To test whether phosphorolysis of pyruvate-derived intermediates could restore OOR activity, 50 mM potassium phosphate (pH 7.4) was added to assays of pyruvate-treated OOR. However, no increase in the rate of oxalate-dependent MV reduction was seen over 1 h, indicating that OOR-catalyzed redox catalysis is "self-contained", i.e., unlike PFOR or pyruvate oxidase (POX) in which oxidation of the radical is coupled to reaction with CoA[20] or phosphate[36] to form acetyl-CoA or acetyl phosphate.

Calculation of the Redox Potentials and pK_a Values for OOR and PFOR Intermediates. To explore the role of the hypothesized DM−TPP, DM−TPP radical, and carboxyl-TPP intermediates in the OOR catalytic cycle, we calculated the redox potentials and pK_a values of protonated and deprotonated forms of these intermediates, as well as those for the corresponding HE−TPP, HE−TPP radical, and acetyl-TPP intermediates in PFOR. Calculating these values for all possible protonation states of each intermediate gives insight into which are likely to be formed during the catalytic cycle and can provide upper and lower limits for the effects of active site amino acid residues on these parameters. For example, if an amino acid residue accepts (donates) a hydrogen bond from (to) the neutral DM−TPP radical, the reduction potential of the intermediate is expected to lie between those calculated for the neutral and anionic (cationic) forms. Figures 6 and 7 show the results of these calculations. Both figures start in the top left corner with the substrate-derived adduct formed in step 2 (DM−TPP or HE−TPP for OOR or PFOR, respectively). Shown in blue are the intermediates that are expected to be relevant to the enzymatic mechanisms, based on the physiological relevance of their pK_a and $E°$ values. One-electron oxidation by the internal electron transfer chain of [4Fe-4S] clusters leads to the protonated DM−TPP or HE−TPP radicals. The calculated redox potentials for these radical intermediates are nearly identical (−0.47 or −0.46 V,

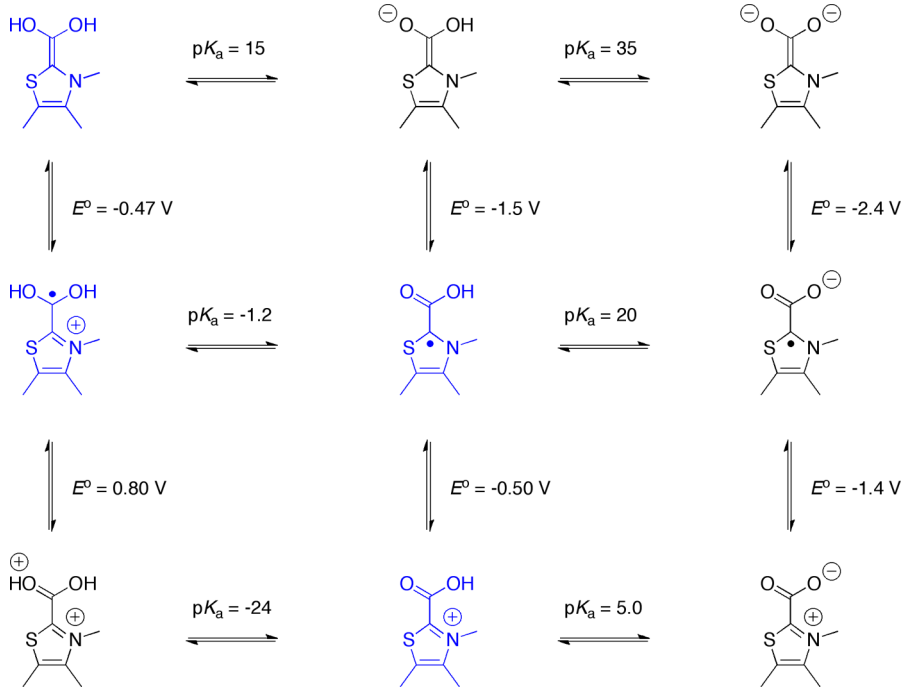

Figure 6. Calculated redox potentials and pK_a values for proposed intermediates in the OOR catalytic cycle. Potentials are vs the standard hydrogen electrode in acetonitrile.

DOI: 10.1021/acs.biochem.7b00222
Biochemistry 2017, 56, 2824−2835

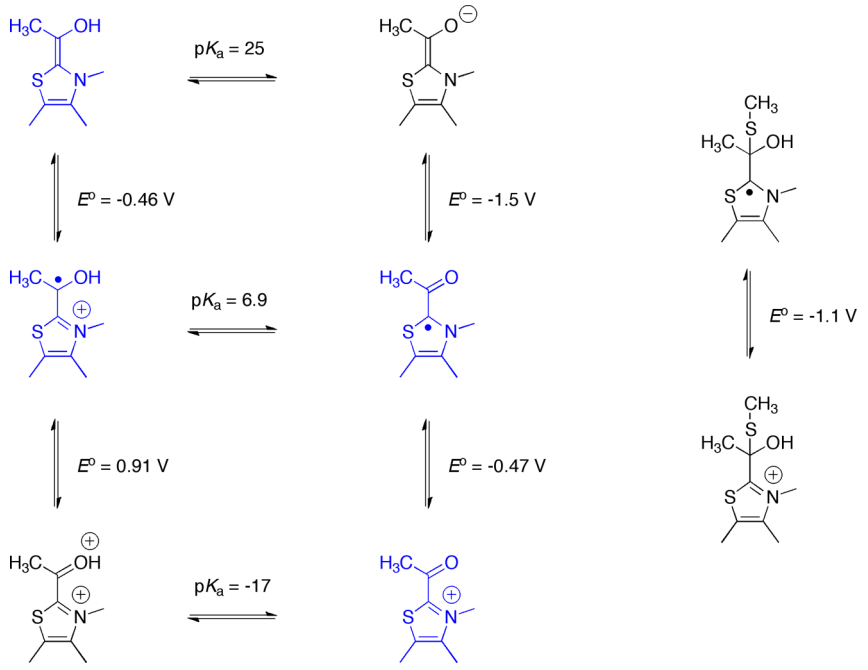

Figure 7. Calculated redox potentials and pK_a values for proposed intermediates in the PFOR catalytic cycle. Potentials are vs the standard hydrogen electrode in acetonitrile.

respectively). These potentials closely match those of the iron−sulfur clusters in PFOR, which have been measured to be between −0.54 and −0.39 V.[37] If the potentials of the OOR iron−sulfur clusters are within a similar range, the reduction potential for the DM−TPP radical intermediate is in the proper range to allow facile electron transfer into this network. As described for PFOR, the electron transfer would occur first to the cluster that is closest to TPP and then to the other clusters, which have a more positive potential, thus reoxidizing the proximal cluster.[37] Once formed, the protonated forms of the DM− and HE−TPP radicals would be unable to transfer an electron into the chain of iron−sulfur clusters because that redox reaction would be unfavorable by >1.3 V. However, the potentials for the redox couples of the deprotonated forms of each radical with carboxyl- and acetyl-TPP once again match the experimental values for the iron−sulfur clusters (−0.50 and −0.47 V, respectively). Interestingly, the calculated pK_a for the HE−TPP radical is in the physiological range (pK_a = 6.9), while the DM−TPP radical is a strong acid (pK_a = −1.2). The difference in pK_a values is likely to be the result of replacing an electron-donating substituent (-CH_3) derived from pyruvate with an electron-withdrawing one (-OH) from oxalate on a cationic acid. Thus, in OOR, the DM−TPP radical intermediate would undergo rapid deprotonation to generate the carboxyl-TPP radical (in the middle of Figure 6), which would then be able to transfer its electron into the iron−sulfur cluster chain to generate carboxyl-TPP. The stable HE−TPP radical in PFOR appears to be a H-bonded form of the neutral radical.[22] The H-bonding would render the potential more positive, thus prolonging the lifetime of this intermediate. Disruption of the H-bond network upon CoA binding would facilitate the second electron transfer and promote the coupled reaction to form acetyl-CoA in lieu of acetate.

Impact of Oxalate on PFOR Catalysis. To determine if oxalate is recognized by PFOR as a substrate or inhibitor, we performed steady state assays in the presence and absence of oxalate. We first determinined the K_m (0.49 ± 0.1 mM) and V_{max} (18.3 ± 0.14 units/mg) values for pyruvate (Figure 8). To determine if oxalate is a substrate, we included 10 mM oxalate

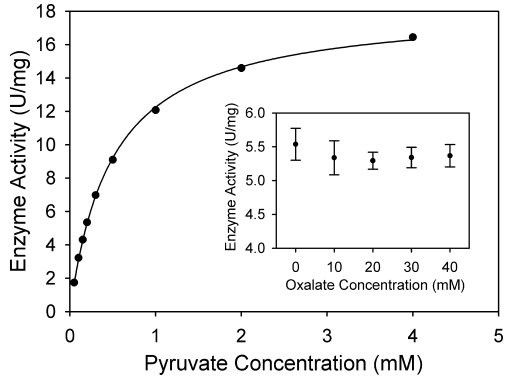

Figure 8. Effect of pyruvate and oxalate on PFOR kinetics. PFOR was reacted with varying concentrations of pyruvate at a saturating CoA concentration to determine the steady state kinetic parameters. Fitting the data to the Michaelis−Menten equation gave K_m and V_{max} values of 0.49 ± 0.1 mM and 18.29 ± 0.14 units/mg, respectively (R^2 = 0.9995). The inset shows PFOR activity at different oxalate concentrations and at a subsaturating pyruvate concentration (0.2 mM). Standard deviations are shown with error bars. No significant changes in activity were observed, showing the oxalate does not inhibit PFOR.

(instead of pyruvate) and found no MV detectable reduction, even with 51 μg of PFOR, which is ∼20-fold larger than what was used in the experiments with pyruvate. Clearly, oxalate does not act as an electron donor for PFOR.

To determine if oxalate can bind to PFOR, we examined its inhibitory properties using 0.2 mM pyruvate in the assays, a concentration that represents k_{cat}/K_m conditions, well below the determined K_m value. As shown in the inset of Figure 8, oxalate does not inhibit pyruvate oxidation by PFOR. Thus, oxalate does not bind competitively with pyruvate to the active site of PFOR.

DOI: 10.1021/acs.biochem.7b00222
Biochemistry 2017, 56, 2824−2835

DISCUSSION

There were two major aims of our work on OOR. We tested the hypothesis that OOR utilizes a substrate-derived radical in its mechanism. Without taking into account the structure of the OOR active site, our calculations indicate that formation of the DM−TPP adduct from the monoanionic form of oxalate is 22.4 kcal/mol more difficult than formation of the corresponding HE−TPP adduct from pyruvate. What steric and electronic factors are engaged by OOR to overcome this energy barrier allowing microbes to derive energy by oxidizing this dicarboxylic acid? OOR is unique among the known 2-oxoacid:ferredoxin oxidoreductases because its catalytic function is entirely CoA-independent. For example, in PFOR, CoA (and perhaps phosphate in POX)[38] stimulates a key electron transfer reaction (involving oxidation of the radical intermediate) by 10^5-fold. Our results indicate that redox and acid−base properties of the DM−TPP radical, which is similar to the HE−TPP radical of PFOR, allow OOR to catalyze the oxidation of this intermediate in the absence of CoA. Furthermore, by comparing the reaction of OOR to that of PFOR, we aimed to better understand the role of CoA in the reactions of PFOR and of the OFOR family in general.

A substrate-derived radical has been hypothesized to be an intermediate in the mechanisms of all enzymes of this family.[39] The electronic structure and the rates of formation and decay of the HE−TPP radical have been well characterized in PFOR.[20,22,37,39] Formation of a radical intermediate is likely in OOR given that the enzyme contains iron−sulfur clusters, which are obligate one-electron acceptors. Thus, we propose that reaction of OOR with oxalate generates an oxalyl-TPP intermediate that is decarboxylated to form the DM−TPP intermediate. Because of the relatively high energy barrier for the formation of the DM−TPP adduct (above), one might question the ability of any nucleophile to react with oxalate. However, like other carboxylic acids, the O atoms of oxalic acid have been shown to undergo exchange in water, and thus, there is chemical precedent for nucleophilic attack on this dicarboxylic acid.[40] Moreover, the active site of OOR contains an additional positively charged residue (Arg31α) in place of Thr31 in PFOR that appears to function together with Arg109α and H-bond donors to facilitate this nucleophilic attack and stabilize the TPP adduct.[17,18] This substitution is crucial for selection of the correct substrate and for engaging the catalytic machinery for reaction. Oxalate is a potent inhibitor of pyruvate utilizing enzymes, especially ones that use the enolate form, including pyruvate kinase[41,42] and pyruvate phosphate dikinase.[43] Thus, it seemed possible that PFOR would catalyze the oxidative degradation of oxalate. However, oxalate not only does not react but also does not even bind competitively with pyruvate to PFOR (Figure 8), demonstrating that electrophilic catalysis in OOR is essential right from the start of the reaction, where the ylide form of enzyme-bound TPP reacts with the substrate. Regardless, nucleophilic attack by the TPP ylide on oxalate is expected to be at least partially rate-limiting during OOR catalysis.

Once the DM−TPP adduct is formed, one electron is then proposed to be transferred into the iron−sulfur cluster network to form a DM−TPP radical intermediate (step 3 of Figure 1), analogous to the HE−TPP radical intermediate in PFOR. Experimental evidence of this radical intermediate is based predominantly on our observation of an EPR signal upon reaction of OOR with pyruvate that is virtually identical to that of the HE−TPP radical formed on PFOR upon reaction with pyruvate. The radical observed on OOR also exhibits a decreased level of hyperfine splitting upon reaction with deuterated pyruvate, similar to what is observed with PFOR. We propose that pyruvate inhibits OOR by forming an adduct with TPP and generating TPP-bound intermediates, including acetyl-TPP, which cannot proceed further in the catalytic cycle. In PFOR, the acetyl-TPP intermediate reacts with CoA to generate acetyl-CoA. However, in OOR, any acetyl-TPP generated by oxidation of the HE−TPP radical cannot react with CoA, leaving the enzyme trapped in an adduct state that cannot undergo enzymatic turnover with oxalate.

The substrate-derived radical was first seen in PFOR and 2-oxoglutarate:ferredoxin oxidoreductase from *Halobacterium salinarum* (*Halobacterium halobium*)[44] and has been found in other OFORs.[45−48] A substrate-derived HE−TPP radical is also an intermediate in the catalytic cycle of *Lactobacillus plantarum* pyruvate oxidase (*Lp*POX), which catalyzes the oxidation of pyruvate, producing CO_2 and acetyl phosphate. In *Lp*POX, the electrons released are transferred from the TPP active site to a flavin adenine dinucleotide cofactor, which is oxidized by molecular oxygen to form H_2O_2.[38] The structure of the HE−TPP radical has been studied in detail by EPR spectroscopy in PFOR from *M. thermoacetica* and by X-ray crystallography of pyruvate-soaked crystals of PFOR from *D. africanus*. On the basis of a bent conformation of TPP and what appeared to be an unusually long bond (1.70−1.95 Å) between the substrate α-carbon and C2 of the thiazolium ring in the crystal structure, it was suggested that the substrate-derived radical is a σ/n-type cation radical with most of the spin density on the substrate α-carbon.[49,50] However, computational studies and EPR spectroscopy using isotopically labeled pyruvate and TPP support a π-type radical that is delocalized over the hydroxyethyl moiety and the thiazolium ring of TPP.[22]

Like other members of this family, OOR binds TPP, which functions as a nucleophile to generate a substrate adduct that is prone to decarboxylation, and three [4Fe-4S] clusters. These clusters act as an electron sink by accepting two electrons, one at a time, that are transferred to ferredoxin, which couples to other redox reactions in the cell. In this respect, it is intriguing to compare OOR to O_2-dependent oxalate decarboxylase, which also utilizes a radical mechanism[51−53] yet generates formate and CO_2 as products instead of 2 mol of CO_2 and two electrons (eq 5). Thus, oxalate decarboxylase does not catalyze a redox reaction; however, it has been proposed to utilize a cryptic redox mechanism in which oxalate and then O_2 bind to the Mn(II)-bound enzyme to generate a bound superoxo−oxalate−Mn(III) species.[53] Superoxo−Mn(III) is thought to serve as an electron sink, accepting an electron to generate a Mn(II)−oxalate radical intermediate poised for C−C bond cleavage and decarboxylation to yield a Mn(II)−formate radical anion; subsequent back electron transfer and protonation of the radical then produce formate.[53] In contrast, on the basis of the mechanistic results described here and elsewhere,[4] combined with crystallographic studies of OOR[17,18] and with studies of related TPP-dependent OFOR systems,[54] it is nucleophilic attack by TPP to generate the DM−TPP intermediate that promotes C−C bond cleavage (decarboxylation) to generate a stabilized CO_2 anion. Low-potential Fe−S clusters then serve as the electron sink in OOR, ensuring that the free energy of decarboxylation is tightly coupled to redox chemistry. These important functional differences between oxalate decarboxylase

DOI: 10.1021/acs.biochem.7b00222
Biochemistry 2017, 56, 2824−2835

and OOR promote oxalate detoxification in aerobic organisms and oxalate respiration in anaerobes like *M. thermoacetica*.

$$C_2O_4^{2-} + H^+ \rightarrow CO_2 + HCOO^- \quad (5)$$

The mechanisms of OOR and PFOR (and other OFOR family members) diverge at step 4, the second electron transfer step. In PFOR, this electron transfer step is coupled to CoA binding, which promotes rapid decay of the HE−TPP radical. On the other hand, CoA has no effect on (and thus is not needed for) the reaction of OOR with oxalate. Decay of the radical also occurs in PFOR in the absence of CoA, but at a rate that is 10^5-fold slower than when CoA is present. Thus, one can only observe this radical when PFOR is reacted with pyruvate alone; addition of CoA causes such a rapid depletion of the radical that it does not accumulate in sufficient quantities to be detected. Similarly, in OOR, no radical intermediate is observed upon reaction with oxalate, indicating that the relative rates of formation and decay of the DM−TPP radical (steps 3 and 4, respectively) are such that it does not accumulate.

Because the OOR reaction is CoA-independent, we have performed computations to compare the PFOR and OOR electron transfer steps and gain insight into (1) the mechanism by which CoA enhances the electron transfer step for all other members of the OFOR family of enzymes and (2) why OOR does not require CoA. One proposed mechanism for CoA-dependent rate enhancement in PFOR (and OFORs other than OOR) is that the thiolate of CoA forms an adduct with the radical intermediate, generating a highly reducing radical anion that could transfer an electron to the [4Fe-4S] clusters,[37] and the same role has been proposed for phosphate in *Lp*POX.[38] Our calculations show that the adduct of the HE−TPP radical with methanethiol is indeed highly reducing (and thus also a high-energy intermediate), with a redox potential of −1.1 V (Figure 7). Although this would provide a 0.6 V driving force for reduction of the clusters, given the values of the redox potential of the iron−sulfur clusters in PFOR, the oxidation of such an adduct radical might lie in the inverted Marcus region and occur slowly.

We suggest an alternative mechanism in which CoA reacts, not with the radical, but with the acetyl-TPP intermediate to form acetyl-CoA. Thus, this represents an EC-type mechanism in which oxidation of the HE−TPP radical is coupled to the nucleophilic attack of CoA on the acetyl group of acetyl-TPP. Our calculations show that this scenario is thermodynamically more feasible than reaction with the radical, as nucleophilic attack of methanethiol on acetyl-TPP is 20 kcal/mol more favorable than on the HE−TPP radical. Moreover, the observed chemical gating of the second electron transfer may be due to the disruption of the H-bonding interactions to the HE−TPP radical upon CoA binding and/or the positioning of the CoA thiolate near the radical center, each of which would decrease its reduction potential and facilitate its oxidation to acetyl-TPP.[20,22] Alternatively, the gating mechanism may be due to the reaction of CoA with a small equilibrium amount of acetyl-TPP that is present. Thus, efficient removal of acetyl-TPP by CoA pulls the net reaction forward.

Calculations of the redox potentials of proposed intermediates in the OOR reaction support the hypothesis that the redox couple of the protonated DM−TPP intermediate and the corresponding DM−TPP radical has a potential that is low enough to drive reduction of the first iron−sulfur cluster. The resulting DM−TPP radical cation, like the protonated HE−TPP radical, would be unable to reduce the chain of iron−sulfur clusters in these proteins. However, unlike the pK_a of the HE−TPP radical, which is in the neutral range, the pK_a of the protonated DM−TPP radical is −1.2. Thus, proton transfer is likely coupled to the first electron transfer, which would generate the neutral DM−TPP radical directly. This neutral radical now has the appropriate reducing power to transfer an additional electron into the chain of iron−sulfur clusters, forming a carboxyl-TPP intermediate in the active site. Therefore, in OOR, the two electron transfer reactions are likely to occur in rapid succession. As a result, the DM−TPP radical is not expected to accumulate to an extent that would allow it to be detected by EPR. Thus, it appears that PFOR and OOR have adopted different strategies for accomplishing the reaction with pyruvate versus oxalate, and this relates to the difference in the pK_a values of the HE−TPP versus the DM−TPP radical, which is due to the effect of replacing the electron-donating methyl substituent with the electron-withdrawing hydroxyl group. This effect is particularly dramatic because the substrate-derived radicals are (at least partially) positively charged and the substituents are bonded directly to an atom that is part of the conjugated π system of the radical.

The C2 group of TPP undergoes deprotonation to form the active ylide that reacts with substrate in step 1 of all TPP-dependent enzymes.[55] These enzymes are known to accelerate C2 deprotonation by a mechanism that involves interaction of a glutamate with N1′ in the pyrimidine ring, which increases the basicity of the 4′-amino group allowing it to act as an efficient acceptor for the C2 proton.[56] Apparently, it is the 1′,4′-iminopyrimidine tautomer of TPP that is poised to generate the reactive ylide/carbene at the thiazolium C2 position.[57] We propose that this same proton transfer network plays a critical role during OFOR catalysis by modulating the stability of the radical intermediates and influencing the rate of the electron transfer steps. In particular, the 4′-amino group and an active site arginine residue (Arg114 in PFOR and Arg109α in OOR) form hydrogen bonding interactions that stabilize the neutral forms of the HE−TPP and DM−TPP radicals, respectively. In PFOR, CoA binding may alter these H-bonding interactions, thereby tuning the reduction potential of the radical (and possibly also the cluster) to facilitate the second electron transfer. However, a different, CoA-independent strategy must be utilized by OOR.

Crystallographic studies of OOR have uncovered important conformational changes in which movement of a switch loop is associated with substrate binding and formation of various intermediates.[18] In the OOR structure with carboxyl-TPP bound (PDB entry 5EXE), ∼50% of the switch loop is in the Asp-in conformation. In forming this Asp-in conformation, Arg109α swings away from its ionic interactions with carboxyl-TPP, observed in the Asp-out state, and Asp112α moves within H-bonding distance of the carboxyl group of carboxyl-TPP (Figure 9). This charge reversal in the active site would be expected to decrease the reduction potential of the carboxyl-TPP/DM−TPP radical couple and facilitate the second electron transfer step. Moreover, this conformational change positions Asp112α such that it can accept a proton from carboxyl-TPP to promote CO_2 formation in step 5 of the OOR mechanism. Interestingly, a loop segment within the active site of *Bacillus subtilis* oxalate decarboxylase is involved in mediating a proton-coupled electron transfer step prior to the decarboxylation step in the mechanism.[58]

The involvement of the switch loop in OOR catalysis also provides an explanation for why the HE−TPP radical formed

DOI: 10.1021/acs.biochem.7b00222
Biochemistry 2017, 56, 2824−2835

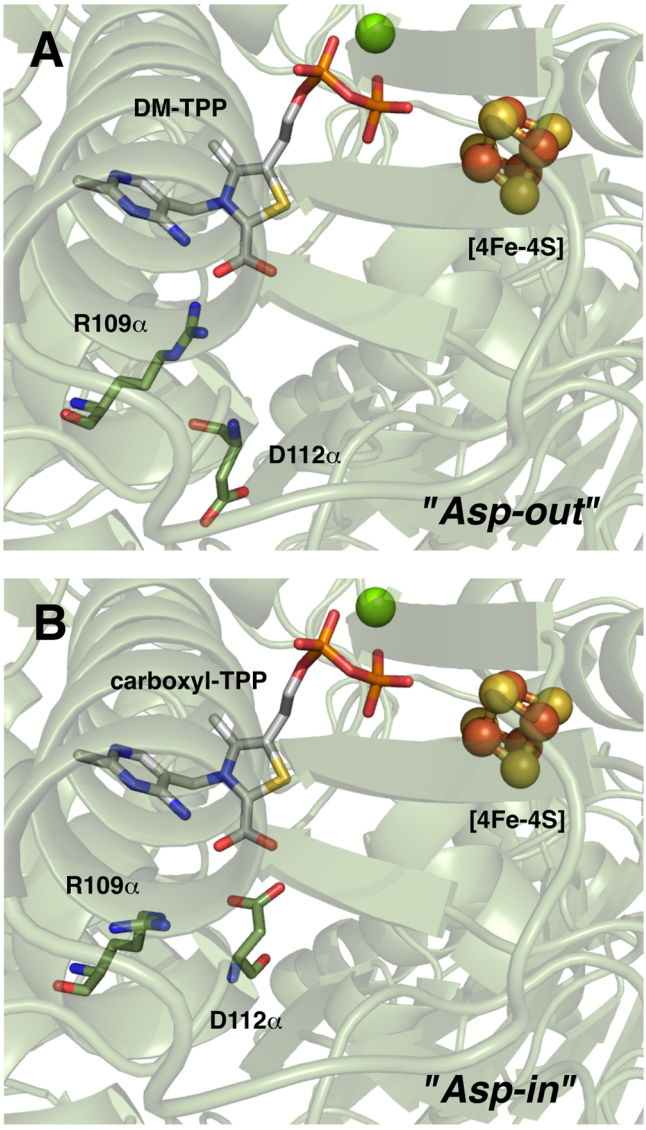

Figure 9. Switch loop in OOR in the (A) "Asp-out" and (B) "Asp-in" conformations. From PDB entry 5EXE.[18] The proximal cluster is shown as brown and yellow spheres, and the Mg^{2+} ion that coordinates the pyrophosphate of TPP is shown as a green sphere.

by pyruvate with OOR does not decay as it does in PFOR. Such a decay would provide a "reactivation" pathway for the pyruvate-inhibited enzyme. Asp112α, which we propose facilitates the release of CO_2 from carboxyl-TPP by serving as a catalytic base, would be unable to accept a proton from acetyl-TPP and thus cannot promote release of the acetyl moiety and regeneration of the TPP ylide as is observed with binding of CoA to PFOR.

AUTHOR INFORMATION

Corresponding Author

*Stephen W. Ragsdale, Department of Biological Chemistry, University of Michigan, 1150 W. Medical Center Dr., Ann Arbor, MI 48109. E-mail: sragsdal@umich.edu. Telephone: (734) 615-4621. Fax: (734) 763-4581.

ORCID

Stephen W. Ragsdale: 0000-0003-3938-8906

Present Address

‖E.P.: Department of Chemistry, Southern Utah University, 351 W. University Blvd., Cedar City, UT 84720.

Author Contributions

S.O.M., G.H.R., and S.W.R. designed the experiments. E.P., S.O.M., and M.C. performed the research and analyzed the data.

Funding

Funding was provided by Grant R37-GM39451 (S.W.R.).

Notes

The authors declare no competing financial interest.

ABBREVIATIONS

CoA, coenzyme A; DM−TPP, dihydroxymethylidene−TPP; DTT, dithiothreitol; EPR, electron paramagnetic resonance; Fe−S, iron−sulfur; HE−TPP, hydroxyethylidene−TPP; MV, methyl viologen; OFOR, 2-oxoacid:ferredoxin oxidoreductase; OOR, oxalate:ferredoxin oxidoreductase; PFOR, pyruvate:ferredoxin oxidoreductase; POX, pyruvate oxidase; TPP, thiamin pyrophosphate.

REFERENCES

(1) Adams, M. W. W., and Kletzin, A. (1996) Oxidoreductase-type enzymes and redox proteins involved in fermentative metabolisms of hyperthermophilic archaea. *Adv. Protein Chem. 48*, 101−180.

(2) Ragsdale, S. W. (2003) Pyruvate:ferredoxin oxidoreductase and its radical intermediate. *Chem. Rev. 103*, 2333−2346.

(3) Daniel, S. L., Pilsl, C., and Drake, H. L. (2004) Oxalate metabolism by the acetogenic bacterium *Moorella thermoacetica*. *FEMS Microbiol. Lett. 231*, 39−43.

(4) Pierce, E., Becker, D. F., and Ragsdale, S. W. (2010) Identification and characterization of oxalate oxidoreductase, a novel thiamine pyrophosphate-dependent 2-oxoacid oxidoreductase that enables anaerobic growth on oxalate. *J. Biol. Chem. 285*, 40515−40524.

(5) Noor, E., Bar-Even, A., Flamholz, A., Lubling, Y., Davidi, D., and Milo, R. (2012) An integrated open framework for thermodynamics of reactions that combines accuracy and coverage. *Bioinformatics 28*, 2037−2044.

(6) Noor, E., Haraldsdottir, H. S., Milo, R., and Fleming, R. M. (2013) Consistent estimation of Gibbs energy using component contributions. *PLoS Comput. Biol. 9*, e1003098.

(7) Franceschi, V. R., and Nakata, P. A. (2005) Calcium oxalate in plants: formation and function. *Annu. Rev. Plant Biol. 56*, 41−71.

(8) Strobel, B. W. (2001) Influence of vegetation on low-molecular-weight carboxylic acids in soli solution - a review. *Geoderma 99*, 169−198.

(9) Whittaker, M. M., and Whittaker, J. W. (2002) Characterization of recombinant barley oxalate oxidase expressed by Pichia pastoris. *JBIC, J. Biol. Inorg. Chem. 7*, 136−145.

(10) Tanner, A., Bowater, L., Fairhurst, S. A., and Bornemann, S. (2001) Oxalate decarboxylase requires manganese and dioxygen for activity. *J. Biol. Chem. 276*, 43627−43634.

(11) Baetz, A. L., and Allison, M. J. (1989) Purification and characterization of oxalyl-coenzyme A decarboxylase from *Oxalobacter formigenes*. *J. Bacteriol. 171*, 2605−2608.

(12) Berthold, C. L., Moussatche, P., Richards, N. G., and Lindqvist, Y. (2005) Structural basis for activation of the thiamin diphosphate-dependent enzyme oxalyl-CoA decarboxylase by adenosine diphosphate. *J. Biol. Chem. 280*, 41645−41654.

(13) Seifritz, C., Fröstl, J. M., Drake, H. L., and Daniel, S. L. (2002) Influence of nitrate on oxalate- and glyoxylate-dependent growth and acetogenesis by *Moorella thermoacetica*. *Arch. Microbiol. 178*, 457−464.

(14) Seifritz, C., Frostl, J. M., Drake, H. L., and Daniel, S. L. (1999) Glycolate as a metabolic substrate for the acetogen Moorella thermoacetica. *FEMS Microbiol. Lett. 170*, 399−405.

DOI: 10.1021/acs.biochem.7b00222
Biochemistry 2017, 56, 2824−2835

(15) Daniel, S. L., and Drake, H. L. (1993) Oxalate- and glyoxylate-dependent growth and acetogenesis by *Clostridium thermoaceticum*. *Appl. Environ. Microbiol. 59*, 3062−3069.
(16) Chabrière, E., Charon, M. H., Volbeda, A., Pieulle, L., Hatchikian, E. C., and Fontecilla-Camps, J. C. (1999) Crystal structures of the key anaerobic enzyme pyruvate:ferredoxin oxidoreductase, free and in complex with pyruvate. *Nat. Struct. Biol. 6*, 182−190.
(17) Gibson, M. I., Brignole, E., Pierce, E., Can, M., Ragsdale, S. W., and Drennan, C. L. (2015) Structure of an oxalate oxidoreductase provides insight into microbial 2-oxoacid metabolism. *Biochemistry 54*, 4112−4120.
(18) Gibson, M. I., Chen, P. Y., Johnson, A. C., Pierce, E., Can, M., Ragsdale, S. W., and Drennan, C. L. (2016) One-carbon chemistry of oxalate oxidoreductase captured by X-ray crystallography. *Proc. Natl. Acad. Sci. U. S. A. 113*, 320−325.
(19) Furdui, C., and Ragsdale, S. W. (2000) The role of pyruvate:ferredoxin oxidoreductase in pyruvate synthesis during autotrophic growth by the Wood-Ljungdahl pathway. *J. Biol. Chem. 275*, 28494−28499.
(20) Furdui, C., and Ragsdale, S. W. (2002) The Roles of Coenzyme A in the Pyruvate:Ferredoxin Oxidoreductase Reaction Mechanism: Rate Enhancement of Electron Transfer from a Radical Intermediate to an Iron-Sulfur Cluster. *Biochemistry 41*, 9921−9937.
(21) Tittmann, K. (2009) Reaction mechanisms of thiamin diphosphate enzymes: redox reactions. *FEBS J. 276*, 2454−2468.
(22) Mansoorabadi, S. O., Seravalli, J., Furdui, C., Krymov, V., Gerfen, G. J., Begley, T. P., Melnick, J., Ragsdale, S. W., and Reed, G. H. (2006) EPR Spectroscopic and Computational Characterization of the Hydroxyethylidene-Thiamine Pyrophosphate Radical Intermediate of Pyruvate:Ferredoxin Oxidoreductase. *Biochemistry 45*, 7122−7131.
(23) Becke, A. D. (1993) Density-Functional Thermochemistry 0.3. The Role of Exact Exchange. *J. Chem. Phys. 98*, 5648−5652.
(24) Becke, A. D. (1993) Density-functional thermochemistry. III. The role of exact exchange. *J. Chem. Phys. 98*, 5648−5652.
(25) Raghavachari, K., Binkley, J. S., Seeger, R., and Pople, J. A. (1980) Self-Consistent Molecular Orbital Methods. 20. Basis set for correlated wave-functions. *J. Chem. Phys. 72*, 650−654.
(26) Andersson, M. P., and Uvdal, P. (2005) New scale factors for harmonic vibrational frequencies using the B3LYP density functional method with the triple-zeta basis set 6-311+G(d,p). *J. Phys. Chem. A 109*, 2937−2941.
(27) Tomasi, J., Mennucci, B., and Cammi, R. (2005) Quantum mechanical continuum solvation models. *Chem. Rev. 105*, 2999−3093.
(28) Tissandier, M. D., Cowen, K. A., Feng, W. Y., Gundlach, E., Cohen, M. H., Earhart, A. D., Coe, J. V., and Tuttle, T. R., Jr. (1998) The Proton's Absolute Aqueous Enthalpy and Gibbs Free Energy of Solvation from Cluster-Ion Solvation Data. *J. Phys. Chem. A 102*, 7787−7794.
(29) Fu, Y., Liu, L., Yu, H. Z., Wang, Y. M., and Guo, Q. X. (2005) Quantum-chemical predictions of absolute standard redox potentials of diverse organic molecules and free radicals in acetonitrile. *J. Am. Chem. Soc. 127*, 7227−7234.
(30) Zhu, X. Q., and Wang, C. H. (2010) Accurate estimation of the one-electron reduction potentials of various substituted quinones in DMSO and CH_3CN. *J. Org. Chem. 75*, 5037−5047.
(31) Karlsson, C., Jämstorp, E., Strømme, M., and Sjödin, M. (2012) Computational electrochemistry study of 16 isoindole-4,7-diones as candidates for organic cathode materials. *J. Phys. Chem. C 116*, 3793−3801.
(32) Karlsson, C., Gogoll, A., Strømme, M., and Sjödin, M. (2013) Investigation of the redox chemistry of isoindole-4,7-diones. *J. Phys. Chem. C 117*, 894−901.
(33) Elliott, J. I., and Brewer, J. M. (1978) The inactivation of yeast enolase by 2,3-butanedione. *Arch. Biochem. Biophys. 190*, 351−357.
(34) Penttinen, H. K. (1979) Fluorometric determination of thiamine and its mono-, di-, and triphosphate esters. *Methods Enzymol. 62*, 58−59.
(35) Jordan, F., and Nemeria, N. S. (2014) Progress in the experimental observation of thiamin diphosphate-bound intermediates on enzymes and mechanistic information derived from these observations. *Bioorg. Chem. 57*, 251−262.
(36) Nemeria, N. S., Ambrus, A., Patel, H., Gerfen, G., Adam-Vizi, V., Tretter, L., Zhou, J., Wang, J., and Jordan, F. (2014) Human 2-oxoglutarate dehydrogenase complex E1 component forms a thiamin-derived radical by aerobic oxidation of the enamine intermediate. *J. Biol. Chem. 289*, 29859−29873.
(37) Astashkin, A. V., Seravalli, J., Mansoorabadi, S. O., Reed, G. H., and Ragsdale, S. W. (2006) Pulsed Electron Paramagnetic Resonance Experiments Identify the Paramagnetic Intermediates in the Pyruvate Ferredoxin Oxidoreductase Catalytic Cycle. *J. Am. Chem. Soc. 128*, 3888−3889.
(38) Tittmann, K., Wille, G., Golbik, R., Weidner, A., Ghisla, S., and Hubner, G. (2005) Radical Phosphate Transfer Mechanism for the Thiamin Diphosphate- and FAD-Dependent Pyruvate Oxidase from Lactobacillus plantarum. Kinetic Coupling of Intercofactor Electron Transfer with Phosphate Transfer to Acetyl-thiamin Diphosphate via a Transient FAD Semiquinone/Hydroxyethyl-ThDP Radical Pair. *Biochemistry 44*, 13291−13303.
(39) Menon, S., and Ragsdale, S. W. (1997) Mechanism of the *Clostridium thermoaceticum* pyruvate:ferredoxin oxidoreductase: Evidence for the common catalytic intermediacy of the hydroxyethylthiamine pyropyrosphate radical. *Biochemistry 36*, 8484−8494.
(40) Lodato, D. T., and Reed, G. H. (1987) Structure of the Oxalate-ATP Complex with Pyruvate Kinase: ATP as a Bridging Ligand for the Two Divalent Cations? *Biochemistry 26*, 2243−2250.
(41) Oria-Hernandez, J., Cabrera, N., Perez-Montfort, R., and Ramirez-Silva, L. (2005) Pyruvate kinase revisited: the activating effect of K+. *J. Biol. Chem. 280*, 37924−37929.
(42) Reed, G. H., and Morgan, S. D. (1974) Kinetic and magnetic resonance studies of the interaction of oxalate with pyruvate kinase. *Biochemistry 13*, 3537−3541.
(43) Michaels, G., Milner, Y., and Reed, G. H. (1975) Magnetic resonance and kinetic studies of pyruvate, phosphate dikinase. Interaction of oxalate with the phosphorylated form of the enzyme. *Biochemistry 14*, 3213−3219.
(44) Cammack, R., Kerscher, I., and Oesterhelt, D. (1980) A stable free radical intermediate in the reaction of 2-oxoacid:ferredoxin oxidoreductases of Halobacterium halobium. *FEBS Lett. 118*, 271−273.
(45) Smith, E. T., Blamey, J. M., and Adams, M. W. W. (1994) Pyruvate ferredoxin oxidoreductases of the hyperthermophilic archaeon, *Pyrococcus furiosus*, and the hyperthermophilic bacterium, *Thermotoga maritima*, have different catalytic mechanisms. *Biochemistry 33*, 1008−1016.
(46) Pieulle, L., Guigliarelli, B., Asso, M., Dole, F., Bernadac, A., and Hatchikian, E. C. (1995) Isolation and characterization of the pyruvate-ferredoxin oxidoreductase from the sulfate-reducing bacterium *Desulfovibrio africanus*. *Biochim. Biophys. Acta, Protein Struct. Mol. Enzymol. 1250*, 49−59.
(47) Mai, X., and Adams, M. W. W. (1994) Indolepyruvate ferredoxin oxidoreductase from the hyperthermophilic archaeon *Pyrococcus furiosus*. *J. Biol. Chem. 269*, 16726−16732.
(48) Heider, J., Mai, X., and Adams, M. W. W. (1996) Characterization of 2-ketoisovalerate ferredoxin oxidoreductase, a new and reversible coenzyme A-dependent enzyme involved in peptide fermentation by hyperthermophilic archaea. *J. Bacteriol. 178*, 780−787.
(49) Chabriere, E., Vernede, X., Guigliarelli, B., Charon, M. H., Hatchikian, E. C., and Fontecilla-Camps, J. C. (2001) Crystal structure of the free radical intermediate of pyruvate:ferredoxin oxidoreductase. *Science 294*, 2559−2563.
(50) Cavazza, C., Contreras-Martel, C., Pieulle, L., Chabriere, E., Hatchikian, E. C., and Fontecilla-Camps, J. C. (2006) Flexibility of thiamine diphosphate revealed by kinetic crystallographic studies of the reaction of pyruvate-ferredoxin oxidoreductase with pyruvate. *Structure 14*, 217−224.

DOI: 10.1021/acs.biochem.7b00222
Biochemistry 2017, 56, 2824−2835

(51) Molt, R. W., Jr., Lecher, A. M., Clark, T., Bartlett, R. J., and Richards, N. G. (2015) Facile C(sp(2))-C(sp(2)) bond cleavage in oxalic acid-derived radicals. *J. Am. Chem. Soc. 137*, 3248−3252.
(52) Reinhardt, L. A., Svedruzic, D., Chang, C. H., Cleland, W. W., and Richards, N. G. (2003) Heavy atom isotope effects on the reaction catalyzed by the oxalate decarboxylase from Bacillus subtilis. *J. Am. Chem. Soc. 125*, 1244−1252.
(53) Zhu, W., Wilcoxen, J., Britt, R. D., and Richards, N. G. (2016) Formation of Hexacoordinate Mn(III) in Bacillus subtilis Oxalate Decarboxylase Requires Catalytic Turnover. *Biochemistry 55*, 429−434.
(54) Reed, G. H., Ragsdale, S. W., and Mansoorabadi, S. O. (2012) Radical reactions of thiamin pyrophosphate in 2-oxoacid oxidoreductases. *Biochim. Biophys. Acta, Proteins Proteomics 1824*, 1291−1298.
(55) Schellenberger, A., and Hübner, G. (1985) Thiamine pyrophosphate — carrier of the catalytic function of C-C-splitting enzymes. *Biochem. Educ. 13*, 160−163.
(56) Kern, D., Kern, G., Neef, H., Tittmann, K., Killenberg-Jabs, M., Wikner, C., Schneider, G., and Hubner, G. (1997) How thiamine diphosphate is activated in enzymes. *Science 275*, 67−70.
(57) Nemeria, N., Chakraborty, S., Baykal, A., Korotchkina, L. G., Patel, M. S., and Jordan, F. (2007) The 1′,4′-iminopyrimidine tautomer of thiamin diphosphate is poised for catalysis in asymmetric active centers on enzymes. *Proc. Natl. Acad. Sci. U. S. A. 104*, 78−82.
(58) Saylor, B. T., Reinhardt, L. A., Lu, Z., Shukla, M. S., Nguyen, L., Cleland, W. W., Angerhofer, A., Allen, K. N., and Richards, N. G. (2012) A structural element that facilitates proton-coupled electron transfer in oxalate decarboxylase. *Biochemistry 51*, 2911−2920.

DOI: 10.1021/acs.biochem.7b00222
Biochemistry 2017, 56, 2824−2835